

Embryonic Pattern Scaling Achieved by Oppositely Directed Morphogen Gradients

Peter McHale, Wouter-Jan Rappel and Herbert Levine

Department of Physics and Center for Theoretical Biological Physics, University of California, San Diego, La Jolla, CA 92093-0374, USA

Abstract. Morphogens are proteins, often produced in a localised region, whose concentrations spatially demarcate regions of differing gene expression in developing embryos. The boundaries of expression must be set accurately and in proportion to the size of the one-dimensional developing field; this cannot be accomplished by a single gradient. Here, we show how a pair of morphogens produced at opposite ends of a developing field can solve the pattern-scaling problem. In the most promising scenario, the morphogens effectively interact according to the annihilation reaction $A + B \rightarrow \emptyset$ and the switch occurs according to the absolute concentration of A or B . In this case embryonic markers across the entire developing field scale approximately with system size; this cannot be achieved with a pair of non-interacting gradients that combinatorially regulate downstream genes. This scaling occurs in a window of developing-field sizes centred at a few times the morphogen decay length.

PACS numbers: 87.18.La 87.10.+e

1. Introduction

Morphogen gradients play a crucial role in establishing patterns of gene expression during development. These patterns then go on to determine the complex three-dimensional morphology that is needed for organism functionality. Because not all environmental variation can be controlled, gene patterning must be robust to a variety of perturbations, i.e. must compensate for the unpredictable [1].

One aspect of this robustness concerns the notion of size scaling [2]. Typically, gene patterns are established in proportion to the (variable) size of the nascent embryo. A dramatic demonstration of this was made recently in the case of *Drosophila* where the posterior boundary of the *hunchback* gene expression domain was shown to scale (to within 5%) with embryo size [3]. In the standard model of pattern formation in developmental biology cells acquire their positional information by measuring the concentration of a morphogen gradient and comparing to some hard-wired set of thresholds [4, 5, 6]. As the simplest single-source diffusing morphogen gradient with fixed thresholds clearly does not exhibit this type of proportionality, it is clear that more sophisticated dynamics must be responsible for the observed structures [7]. Unfortunately, little to nothing is known experimentally about how this pattern scaling comes about.

As a first step in deciphering what these more complex processes might entail, we study here the issue of how two morphogen gradients, directed from opposite ends of a developing field, may solve the pattern-scaling problem [4]. Operationally, opposing gradients may arise in developing systems in at least two ways. First mRNA, from which protein is translated, may be anchored at opposite ends of the region in question. As an example, in the *Drosophila* syncytium an anterior-to-posterior gradient is established by the localisation of *bicoid* mRNA to the anterior, while *nanos* mRNA localised at the posterior defines a reciprocal gradient [8]. Second, protein may be secreted by clusters of cells, one cluster located at opposite ends of the developing field [9]. In both cases we will assume that there is some flux of morphogens entering a specific region and assume that there is no production in the bulk of the region. We further assume that the morphogen reaches neighbouring cells by an effective diffusion process thereby creating a gradient [10]. Finally, although time-dependent effects in development patterning might be important in some contexts [11], we assume here that a steady-state analysis is sufficient insofar as scaling of patterns with system size is concerned.

We consider two mechanisms in which a pair of morphogen gradients transmits size information to the developmental pattern. The first mechanism, which uses the concentrations of both gradients combinatorially, is an alternative to the simple gradient mechanism [12]. In this mechanism there exist overlapping DNA-binding sites of species *A* and *B* in the cis-regulatory modules of the target genes. We note that in the *Drosophila* syncytium some *krüppel* binding sites overlap extensively with *bicoid* sites [12, 13]. In this scenario one of the morphogens acts as a transcription factor and the other acts as an effective repressor by occluding the binding site of the first. Hence the

target gene is switched on according to the relative concentrations of the two species [14]. In the second mechanism protein B irreversibly inhibits the activity of transcription factor A by either directly degrading it or by irreversibly binding to it. The interaction is described by the annihilation reaction $A + B \rightarrow \emptyset$. Here we assume that the target gene measures the absolute value of the A concentration as in the standard model of developmental patterning; the B gradient serves only to provide size information to the A concentration field.

The goal of this work is to study these two possibilities and see the extent to which they do in fact solve the pattern scaling problem. To this end we measure the range of variables over which scaling is approximately valid. We begin in § 2 by pointing out that a single gradient in a finite system cannot set markers proportionately in the developing field. In § 3 we study the case of two gradients whose binding sites overlap and show that approximate scaling then occurs in a restricted fraction of the developing field typically located midway between the sources. We then turn to the annihilation model of two gradients in § 4 and show that its scaling performance is excellent throughout the developing field.

2. Single Gradient

Let A be the concentration of the morphogen which in the simplest model obeys

$$0 = D_a \partial_x^2 A - \beta_a A \quad (1)$$

at steady state. Here D_a is the diffusion constant of protein A and β_a is the degradation rate. Molecules of A are injected at the left boundary with rate Γ_a and are confined to the interval $[0, L]$ by a zero-flux boundary condition

$$-D_a \partial_x A(0) = \Gamma_a; \quad -D_a \partial_x A(L) = 0. \quad (2)$$

The obvious solution is

$$A = \frac{\lambda_a \Gamma_a}{D_a} \left[\sinh \left(\frac{L}{\lambda_a} \right) \right]^{-1} \cosh \left(\frac{L-x}{\lambda_a} \right) \equiv A(L) \cosh \left(\frac{L-x}{\lambda_a} \right). \quad (3)$$

The length scale λ_a is defined by $\lambda_a = \sqrt{D_a/\beta_a}$.

Let us assume that the boundary between different gene expression regions is determined by the position x_t at which A equals some threshold value A_t . Inverting, the expression for the threshold position is

$$x_t(L) = L - \lambda_a \cosh^{-1} (A_t/A(L)). \quad (4)$$

Note that there is a minimum system size for a specific threshold,

$$L_m = \lambda_a \sinh^{-1} \left(\frac{\lambda_a \Gamma_a}{D_a A_t} \right), \quad (5)$$

such that $x_t(L_m) = L_m$. When $L - x_t \gg \lambda_a$ the concentration profile becomes purely exponential and $x_t \rightarrow x_\infty$ where

$$x_\infty = \lambda \ln \left(\frac{\lambda_a \Gamma_a}{D_a A_t} \right). \quad (6)$$

Clearly, the function $x_t(L)$ starts out at L_m (which is greater than x_∞), is monotonically decreasing, but is bounded below by x_∞ ; in other words x_t is always greater than x_∞ as the effect of the zero-flux boundary condition is to make x_t larger than it would be in the absence of the boundary. Fig. 1 shows the variation of x_t/L with L for three different values of the threshold concentration A_t . There is no extremum where this ratio becomes locally L -independent.

3. Combinatorial model

We next ask whether a molecular mechanism, which compares the concentrations of two gradients rather than reading the absolute value of one or both of them, can lead to gene expression boundaries which scale with system size. We consider two opposing gradients A and B described by

$$0 = D_a \partial_x^2 A - \beta_a A \quad (7)$$

$$0 = D_b \partial_x^2 B - \beta_b B \quad (8)$$

at steady state. The boundary conditions are

$$\begin{aligned} -D_a \partial_x A(0) &= \Gamma_a; & -D_a \partial_x A(L) &= 0 \\ -D_b \partial_x B(0) &= 0; & -D_b \partial_x B(L) &= -\Gamma_b. \end{aligned} \quad (9)$$

In this scenario, the gene expression boundary will be determined by a critical concentration ratio r which occurs at the position x_r defined by $A(x_r) = rB(x_r)$.

Just as in the one-gradient case, one can distinguish between relatively small systems (for which the no-flux boundary conditions matter) and large systems, depending on how big L is compared to the decay lengths λ_i . For sufficiently large L , the gradients of A and B are purely exponential, $A = A(0) \exp(-x/\lambda_a)$ and $B = B(L) \exp(-(L-x)/\lambda_b)$, and the gene expression boundary is given by

$$x_r = \frac{\lambda_a}{\lambda_a + \lambda_b} (L \pm L_c) \quad (10)$$

where

$$L_c = \lambda_b \left| \ln \left(\frac{rB(L)}{A(0)} \right) \right|. \quad (11)$$

Consider a gene whose cis-regulatory module contains overlapping A and B binding sites. This gene will have a particular threshold ratio r and a concomitant value $L_c(r)$. Then for sufficiently large developing fields $L \gg L_c(r)$ the combinatorial mechanism sets the boundary of expression of the gene at the relative location

$$\frac{x_r}{L} = \frac{\lambda_a}{\lambda_a + \lambda_b} \quad (12)$$

in a size-invariant manner. This position is also insensitive to source-level fluctuations, which only enter in L_c . In a system in which the degradation lengths of the two morphogen gradients are comparable, x_r/L will be close to $1/2$.

Although this model can achieve some degree of size-scaling near the centre of the developing field, from Eq. (10) it is clear that the variation of x_r/L with L increases as x_r/L deviates from the aforementioned asymptotic value. This will happen either as the size of the system is made smaller, or even at fixed L if we try to make the threshold point x_r approach the edges of the developing field. We have in mind a situation where multiple genes need to be regulated, each at different points along the developing field; each gene will have its own value of r and hence its own value of x_r . In the previous limit, there is no variation in x_r with r and this cannot be accomplished; therefore we need to rely on finite L_c/L effects. To proceed, we must more carefully characterize the variation of x_r/L with L for all positions in the developing field. Since Eq. (10) becomes inaccurate close to the edges of the developing field we return to the expression for A in Eq. (3) (and a similar one for B) and obtain the following implicit equation for x_r

$$\frac{A(L)}{\cosh(x_r/\lambda_a)} = \frac{rB(0)}{\cosh((L-x_r)/\lambda_b)} \quad (13)$$

valid for a finite system. It will be critical to identify what happens to x_r when the length L is made smaller. Notice that there is a different behavior depending on which of $A(L)$ and $rB(0)$ is larger. Specifically, if $A(L)$ is larger, there will be a smallest length below which x_r given by this formula becomes larger than L ; this length is given by

$$L^*(r) = \lambda_a \cosh^{-1} \left(\frac{A(L)}{rB(0)} \right).$$

If, on the other hand, the ordering is reversed, below the length scale

$$L^*(r) = \lambda_b \cosh^{-1} \left(\frac{rB(0)}{A(L)} \right)$$

we obtain negative values for x_r . Representative x_r/L curves are shown in Fig. 2 for the case of equal decay lengths $\lambda_a = \lambda_b$.

Consider now a developing field of size L subject to a natural variation in size of $L \pm pL$ with $0 \leq p \leq 1$. The variation in the fractional position at which a gene is turned on is then given by

$$\delta \left(\frac{x_r}{L} \right) \equiv \frac{x_r(L-pL)}{L-pL} - \frac{x_r(L+pL)}{L+pL}. \quad (14)$$

We show in Fig. 3(a), again for the equal decay length case, the dependence of $\delta(x_r/L)$ on normalised position x_r/L in the developing field for $L = 4$. As expected the variation is largest (in magnitude) at the boundaries and vanishes at that position x_{r_0} for which the critical length $L_c(r_0)$ vanishes. Defining an arbitrary scaling criterion according to

$$\delta(x/L) \leq 5\%, \quad (15)$$

one sees that the combinatorial model achieves scaling only in the central region of the developing field between about 30% and 70% of L .

Near the edges of the developing field the variation $\delta(x_r/L)$ is about 14%. Since the slopes of the x_r/L curves at $x_r/L = 1$ become flatter as L is increased (see Fig. 2),

one might wonder whether operating at larger system sizes will decrease this variation. However at larger system sizes the flattening effect is offset by the fact that one must sample larger and larger portions of the x_r/L curve. The extent to which these effects cancel is shown in Fig. 3(b) where we show the variation $\delta(x_r/L)$ closest to the right boundary of the developing field as a function of L . The variation decreases with L , but an elementary calculation reveals that it has the lower bound $p/(1+p)$. For a percentage variation $p = 10\%$ in system size this lower bound is about 9%. We conclude that increasing system size is not sufficient to make the combinatorial model, with $\lambda_a = \lambda_b$, meet the scaling criterion throughout the developing field.

A further difficulty with the combinatorial model is its susceptibility to small-molecule-number fluctuations. In general, we must expect L_c of order λ , since we cannot independently adjust the morphogen sources for the multiple genes that need to be controlled. In fact, the natural interpretation of r as being due to binding differences between different transcription factors suggest that L_c would vary significantly. In such cases the limit $L \gg L_c(r_0)$ would force the comparison point x_r far down the profile from the source; having enough molecules at this point to affect the necessary DNA binding would then place a severe constraint on source strengths. In this regard a combinatorial mode of action may favour power-law (resulting e.g. from nonlinear degradation [15]) over exponential profiles as the former have greater range than the latter, but this remains to be studied.

4. Annihilation model

We return to the standard model of morphogenesis in which cell-fate boundaries are determined according to the position at which a single morphogen crosses a threshold concentration. We couple this gradient to an auxiliary gradient directed from the opposite end of the developing field. We then ask under what conditions the primary gradient may scale with system size.

We consider two species of morphogen, A and B , in a one-dimensional system of length L with A s and B s injected at opposite ends of the system. The boundary conditions are as in § 3. The species interact according to the annihilation reaction $A+B \rightarrow \emptyset$. In a mean-field description the kinetics is described by the reaction-diffusion equations

$$\partial_t A = D_a \partial_x^2 A - \beta_a A - kAB \quad (16)$$

$$\partial_t B = D_b \partial_x^2 B - \beta_b B - kAB \quad (17)$$

where k is the annihilation rate constant. Later, we will consider more complex models which incorporate non-linear degradation or non-linear (i.e. concentration-dependent) diffusion.

This system of equations, with fluxes $\Gamma_a = \Gamma_b = \Gamma$ and without any decay, was considered by Ben-Naim and Redner [16]. They determined the steady-state spatial distribution of the reactants and of the annihilation zone which they chose

to be centred in the interval $[0, L]$. The annihilation zone is roughly the support of $R(x) = kA(x)B(x)$ or, put another way, that region where the concentration of both species is appreciable. With the aid of a rate-balance argument, they showed that the width w of the annihilation zone scales as $\Gamma^{-1/3}$ and that the concentration in this zone is proportional to $\Gamma^{2/3}$ when $w \ll L$.

Our goal is to understand the relation of the steady-state concentration profiles to the system length L . It is convenient to identify the point x_e in the annihilation zone where the profiles cross, $A(x_e) = B(x_e)$. In the original Ben-Naim—Redner model, the reaction-diffusion equations yield no unique value for x_e ; instead x_e can lie anywhere in the interval $[0, L]$ depending on the choice of initial condition. To see this consider the following rate-balance argument. Since the particles annihilate in a one-to-one fashion the flux of each species into the annihilation zone must be equal. But this condition does not determine x_e uniquely because these fluxes are always equal to the input fluxes at the boundaries. Similarly, the model without degradation cannot support steady states with unequal boundary fluxes. If, however, we now add degradation terms to the steady-state equations, then the flux of each species into the annihilation zone is the flux into the system less the number of degradation events that happen before reaching the zone. Thus, the flux of each species into the annihilation zone now depends on the location x_e and so there is only one value of x_e which balances the fluxes. As we will see, our models will always contain unique steady-state solutions.

A rough estimate of the concentration in the annihilation zone and of the width of the zone can be obtained using the original Ben-Naim—Redner rate-balance argument [16]. We identify three spatial regions: the first where A is in the majority; the second the annihilation zone; and the third where A is in the minority. Assume the concentration of A s in this latter region is negligible compared with that in the other two regions. The concentration of A s in the annihilation zone should then be of the order of the slope of the concentration profile in the annihilation zone times the width w . The slope of the A profile in this region is proportional to j_e/D_a , where j_e is the equal flux of A s or B s into the annihilation zone. Therefore the concentration in the annihilation zone $A_e = A(x_e)$ is

$$A_e \sim j_e w / D_a. \quad (18)$$

If we ignore the loss of A particles in the annihilation zone (valid for small w), then the number of annihilation events per unit time $kA_e^2 w$ should equal the flux j_e . Balancing these two rates gives $j_e \sim k(j_e w / D_a)^2 w$. Hence the width of the annihilation zone scales as

$$w \sim \left(\frac{D_a^2}{j_e k} \right)^{1/3}. \quad (19)$$

In what follows, we will be mostly interested in taking k large enough to give a very small w .

5. The high-annihilation-rate limit

We now explicitly assume that the parameters lie in the limit where $w \ll \min\{x_e, L-x_e\}$. This limit has the considerable advantage that the A - B system may be decoupled by replacing the coupling term kAB by a zero-concentration boundary condition at x_e . In this approximation the concentration of the A subsystem satisfies

$$0 = D_a \partial_x^2 A - \beta_a A \quad (20)$$

subject to the boundary conditions $-D_a \partial_x A(0) = \Gamma_a$ and $A(x_e) = 0$. The solution to this equation is

$$A(x) = \frac{\lambda_a \Gamma_a}{D_a \cosh(x_e/\lambda_a)} \sinh\left(\frac{x_e - x}{\lambda_a}\right) = A_* \sinh\left(\frac{x_e - x}{\lambda_a}\right) \quad (21)$$

where as before $\lambda_a = \sqrt{D_a/\beta_a}$. A_* is a characteristic concentration of the A field related to the slope of the A field at x_e according to $A_* = -\lambda_a \partial_x A(x_e)$. The flux of A particles is

$$j_a(x) = j_a(x_e) \cosh\left(\frac{x_e - x}{\lambda_a}\right). \quad (22)$$

where the flux into the annihilation zone $j_a(x_e)$ is given by $j_a(x_e) = \Gamma_a / \cosh(x_e/\lambda_a)$. Substituting this into Eq. (19) yields the scaling function of the annihilation zone width for the case of linear degradation

$$w \sim w_0 [\cosh(x_e/\lambda_a)]^{1/3}. \quad (23)$$

Here $w_0 \sim (D_a^2/\Gamma_a k)^{1/3}$ is the width of the annihilation zone in the absence of degradation [16]. Note that we may also substitute this expression for $j_a(x_e)$ into Eq. (18) obtaining $A_e \sim w / \cosh(x_e/\lambda_a)$. One can then verify that A_e is much smaller than $A(0)$ whenever $w \ll x_e$ and hence approximating this as a zero boundary condition is self-consistently valid.

The B -subsystem can be treated similarly, except that the length of the subsystem in this case is $L - x_e$. The only dependence on the annihilation rate k in the inequality $w \ll x_e$ occurs in w_0 . Hence this limit is equivalent to the high-annihilation-rate limit $k \gg k_0$, where the threshold value k_0 of the annihilation rate is given by

$$k_0 \sim \frac{D_a^2 \cosh(x_e/\lambda_a)}{\Gamma_a \lambda_a^3 (x_e/\lambda_a)^3}. \quad (24)$$

We determine the annihilation zone location by balancing fluxes into the zone, $j_a(x_e) = -j_b(L - x_e)$. This leads to the following equation for x_e

$$\frac{\Gamma_a}{\cosh\left(\frac{x_e}{\lambda_a}\right)} = \frac{\Gamma_b}{\cosh\left(\frac{L-x_e}{\lambda_b}\right)}. \quad (25)$$

In the special case $\lambda_a = \lambda_b$ this equation coincides with the implicit definition of x_r (with $r = 1$) which arose in the combinatorial model (see Eq. (13)). As in that model there is a smallest length L^* defined by

$$L^* = \lambda_a \cosh^{-1}\left(\frac{\Gamma_a}{\Gamma_b}\right)$$

if $\Gamma_a > \Gamma_b$ and by

$$L^* = \lambda_b \cosh^{-1} \left(\frac{\Gamma_b}{\Gamma_a} \right)$$

if the flux ordering is reversed. As our entire treatment of the annihilation zone only makes sense if $0 \leq x_e \leq L$, we must always choose $L > L^*$. A comparison of the numerical solution of the full model with the results of the large-annihilation-rate approximation is shown in Fig. 4.

Once we know $x_e(L)$ and $A(x)$, we can proceed to determine the qualitative features of the $x_t(L)$ function with a view to identifying the region of system sizes where $x_t \sim L$. Inverting Eq. (21) we find

$$x_t = x_e - \lambda_a \sinh^{-1} \eta \quad (26)$$

where

$$\eta = A_t/A_*. \quad (27)$$

Note that x_t depends on L only through its dependence on x_e and the function $x_t(x_e)$ is monotonically increasing. Obviously $x_t \leq x_e$. In the limit of sufficiently large x_e , we can replace the inverse hyperbolic function with a logarithm and obtain the simpler form

$$x_t \approx x_e - \lambda_a \ln(2\eta). \quad (28)$$

Here, $\eta \approx \frac{A_t}{A(0)} \frac{1}{2} e^{x_e/\lambda_a}$, and x_t approaches its asymptotic value $x_\infty \approx \lambda_a \ln(A(0)/A_t)$ from below. This is of course the answer one would obtain in the absence of any auxiliary gradient.

Now, imagine reducing L and hence x_e from its just-mentioned asymptotic regime and plotting the ratio x_t/L . For the case $\Gamma_a > \Gamma_b$, x_e will eventually hit L followed shortly thereafter by x_t/L hitting unity. There is no reason why this curve should exhibit a maximum, and a direct numerical calculation for $k = 100$ (shown in Fig. 5) verifies this assertion. The situation is dramatically different, however, for the case of $\Gamma_b > \Gamma_a$. Now x_e must approach zero, implying that at some larger L we have $x_t=0$. The curve x_t/L now exhibits a maximum, as is again verified by direct numerical calculations using both the large-annihilation-rate approximation and also just solving the initial model with no approximations whatsoever (see Fig. 6). Near the peak of the curve we have scaling with system size. For completeness, we also present in Fig. 7 the results for equal fluxes.

To compare the scaling performance of the annihilation model with that of the combinatorial model we show in Fig. 8 the dependence of the variation $\delta(x_t/L)$ on normalised position x_t/L in the developing field for $L = 4$. One sees that, according to our scaling criterion in Eq. (15), the annihilation mechanism can easily set markers scale-invariantly throughout a developing field whose size is a few decay lengths. Furthermore at such system sizes a range of threshold values spanning two orders of magnitude ($A_t = 0.01 - 0.7$) is sufficient to cover the entire developing field (see Fig. 7). Such a modest variation in concentration makes the annihilation model less susceptible to small-molecule-number fluctuations than the combinatorial model.

6. Discussion

We have considered two scenarios in which a pair of oppositely directed morphogen gradients are used to set embryonic markers in a size-invariant manner. In the simplest scenario, in which the gradients interact only indirectly through overlapping DNA-binding sites, exponentially distributed fields achieve perfect size scaling at a normalised position $\lambda_a/(\lambda_a + \lambda_b)$ determined only by the morphogen decay lengths λ_a and λ_b . For equal decay lengths, the accuracy with which this model can set markers size-invariantly decreases as the boundaries of the developing field are approached. At the boundaries the accuracy can be no better than $\delta(x_r/L) = p/(1 + p)$ where p is the percentage variation of the field size. In the second model A and B are coupled via the reaction $A + B \rightarrow \emptyset$ and the embryonic markers are set by a single gradient with the second gradient serving only to provide size information to the first. In this scenario, it is easy to arrange parameters such that scaling occurs with an accuracy $\delta(x_t/L)$ better than 5% over the entire developing field for field sizes of only a few decay lengths.

In practice a given morphogen may play both roles in patterning, setting markers in a strictly concentration-dependent manner at some locations in the developing field and in a combinatorial fashion at other locations [12]. The annihilation model naturally sets markers via the gradient whose source is closest to the marker [17], whereas the combinatorial model is better suited to setting markers in the vicinity of the midpoint of the developing field where the variation $\delta(x_r/L)$ is smallest. As the variation $\delta(x/L)$ has a qualitatively different dependence on x/L in either case, a measurement of this curve in a developmental system may distinguish between the mechanisms.

The origin of the scaling form $f(x/L)$ which arises in the strong-coupling limit of the annihilation model is the effective boundary condition $A(x_e) = 0$. In the case $\Gamma_b > \Gamma_a$ (see Fig. 6) the x_t/L curve has a maximum because at small L ($L \sim L_*$) it tends to zero along with x_e/L while at large L ($L \gg L_*$) it is bounded above by x_∞/L . In the $k \ll k_0$ limit, on the other hand, the zero-concentration effective boundary condition is replaced by a zero-flux boundary condition $j_a(L) = 0$ which can never induce the $x_t \sim L$ scaling.

This approach makes it clear why the scaling occurs at intermediate values of L . Once we reach the non-overlapping limit where the two fields do not effectively communicate, the threshold is set by the A profile alone; we have already seen that this cannot give any scaling. For L too small, the annihilation-zone width w becomes comparable to x_e , there is no effective boundary condition and again scaling fails. In fact, if one looks at the expression for w/x_e , namely

$$\frac{w}{x_e} \sim \frac{w_0}{\lambda_a} \left(\frac{\cosh(x_e/\lambda_a)}{(x_e/\lambda_a)^3} \right)^{1/3}, \quad (29)$$

(where $w_0 \sim (D_a^2/\Gamma_a k)^{1/3}$) one sees that the maximum in x_t/L occurs close to the minimum of w/x_e which is reached at $x_e/\lambda_a \approx 3$.

So far we have used linear degradation and simple diffusion in the annihilation model. However, it should be clear from the above arguments that in fact this mechanism

is rather robust to changing the nature of the individual gradients. For example, let us consider quadratic degradation. In the limit that the system size is so big as to render the coupling term kAB irrelevant the A and B profiles reduce to power laws, $A = a/(x + \epsilon_a)^2$ and $B = b/(L - x + \epsilon_b)^2$. The corresponding L -independent threshold position x_∞ is given by

$$x_\infty = \epsilon_a \left(\sqrt{\frac{A(0)}{A_t}} - 1 \right). \quad (30)$$

An argument, similar to one presented earlier for linear degradation, reveals the fact that x_e will be forced to zero for sufficiently small L if $\Gamma_b > \Gamma_a$; this indicates again that to the extent we can believe the large-annihilation-rate approximation, there will be a maximum in the x_t/L curve. This is illustrated for one specific choice of parameters in Fig. 9(a). The maximum again takes place roughly where L becomes so small as to cause the annihilation-zone width to approach x_e . Repeating the derivation of w outlined in § 5 but using a power law instead of hyperbolic sine we obtain

$$\frac{w}{x_e} \sim \frac{w_0}{\epsilon_a} \left(1 + \frac{1}{x_e/\epsilon_a} \right). \quad (31)$$

This expression is a good qualitative description of the exact w/x_e shown in Fig. 9(a) and diverges when $L \rightarrow 0$ as in the case of linear degradation. Notice that scaling is lost when $w \rightarrow x_e$ even though the rate of the annihilation reaction becomes large (Fig. 9(b)). Finally, one can also ask about the effect of making the diffusion constant concentration dependent. This type of effect can arise whenever the morphogen reversibly binds to buffers that differ in mobility from the pure molecule. Fig. 10 illustrates the behavior under the simplest assumption, namely that the diffusion constant varies linearly with concentration for both the A and B fields. Aside from sharpening the transition from the asymptotic non-interacting regime to the regime where x_e approaches zero (as L is lowered), the basic phenomenology is unchanged.

The focus of our work has been the scaling issue. However, we should not lose track of the other requirement for developmental dynamics, namely that the system be relatively robust to fluctuations in parameters such as source fluxes. Fig. 11(a) presents data regarding the variation of x_t with Γ_a and Γ_b in the annihilation model. For simplicity the data is presented for the case of equal decay lengths, $\lambda_a = \lambda_b = \lambda$. The basic conclusion is that the coefficient of variation χ_i , defined as

$$\frac{\delta x_t}{\lambda} = \begin{cases} \chi_a \frac{\delta \Gamma_a}{\Gamma_a} \\ -\chi_b \frac{\delta \Gamma_b}{\Gamma_b} \end{cases}, \quad (32)$$

starts at 1/2 at $A_t = 0$ and then asymptotes to either 1 for variations in Γ_a or zero for variations in Γ_b . These asymptotic values are of course precisely the results obtained for the one-exponential-gradient model. The fact that the χ_i at small x_t is 1/2 can be understood by noting that in this limit x_t is just x_e , which can easily be shown to be approximately (i.e. for large enough L) given by $x_e \approx 0.5(L \pm L_c)$ with

$L_c = \lambda |\ln(\Gamma_b/\Gamma_a)|$. With this approximation for x_e and taking differentials of x_t we obtain

$$\chi_a = \frac{1}{2} + \frac{\eta}{\sqrt{1+\eta^2}} \left[1 - \frac{1}{2} \tanh\left(\frac{x_e}{\lambda}\right) \right], \quad (33)$$

$$\chi_b = \frac{1}{2} \left[1 - \frac{\eta}{\sqrt{1+\eta^2}} \tanh\left(\frac{x_e}{\lambda}\right) \right] \quad (34)$$

where, as before, $\eta = A_t/A_*$. These are good approximations at all values of η for percentage variations in source fluxes as large as 5% (see Fig. 11(a)). The reduction of the χ values from unity represent an increase in system robustness as compared with the single-exponential-gradient model, albeit with a new sensitivity to the B gradient. For comparison we also show in Fig. 11(b) the coefficient of variation which arises in the single-gradient model. The approximation to χ_a in this case is given by

$$\chi_a = \frac{\eta}{\sqrt{\eta^2 - 1}} \quad (35)$$

where now η is defined by $\eta = A_t/A(L)$. Notice that the effect of the boundary ($\eta \downarrow 1$) is to increase the sensitivity of the gradient to variations in the source flux over that for a simple exponential.

7. Conclusions

In this paper we have shown that coupling two oppositely directed morphogen gradients allows patterns to be set in approximate proportion to the size of the developing field. We have considered two coupling mechanisms, the most effective of which couples the gradients via a phenomenological annihilation reaction. Such a mechanism can set boundaries of gene expression across the developing field with a small sample-to-sample variation in the normalised position of the boundaries. In this scenario, there is no magic bullet which ensures either exact scaling or complete robustness. Instead, the effective boundary condition created by the annihilation reaction allows for approximate scale invariance to emerge in one reasonably-sized range of parameter space and similarly lowers the sensitivity of any threshold to source-level fluctuations. Presumably, one could obtain even more robustness and scaling, and possibly even temperature compensation (see for example Ref. [18]), via the introduction of yet additional interactions.

After completion of this work we became aware of similar work in which the annihilation model was applied to pattern scaling in the early *Drosophila* embryo [19, 20]. In contrast to the numerical analysis carried out by the authors of Ref. [20] for the specific case of the *bicoid* morphogen, we have presented here a more general analytic framework which allows for a natural explanation of pattern scaling at intermediate developing-field sizes and of filtration of source-level fluctuations. In particular our work provides an explanation for the fact that they found pattern scaling at L approximately 4-5 times the decay length λ . We note that recent work showing that only *bicoid* binding sites

are needed for scaling provides further support for an annihilation mechanism in the *bicoid-hunchback* problem [21].

Acknowledgments

This work has been supported in part by the NSF-sponsored Center for Theoretical Biological Physics (grant numbers PHY-0216576 and PHY-0225630). PM acknowledges useful discussions with E. Levine, T. Hwa and A. Eldar.

References

- [1] A. Eldar, B.-Z. Shilo, and N. Barkai. *Curr. Opin. Gen. Dev.*, 14:435, 2004.
- [2] T. Gregor, W. Bialek, R.R. de Ruyter van Steveninck, D.W. Tank, and E.F. Wieschaus. *Proc. Natl. Acad. Sci. USA*, 102:18403, 2005.
- [3] B. Houchmandzadeh, E. Wieschaus, and S. Leibler. *Nature*, 415:798, 2002.
- [4] L. Wolpert. *J. Theor. Biol.*, 25:1, 1969.
- [5] W. Driever and C. Nüsslein-Volhard. *Cell*, 54:95, 1988.
- [6] U. Gerland, J.D. Moroz, and T. Hwa. *Proc. Natl. Acad. Sci. USA*, 99:12015, 2002.
- [7] T. Aegerter-Wilmsen, C.M. Aegerter, and T. Bisseling. *J. Theor. Biol.*, 234:13, 2005.
- [8] A. Ephrussi and D. St Johnston. *Cell*, 116:143, 2004.
- [9] A. Eldar, R. Dorfman, D. Weiss, H. Ashe, B.Z. Shilo, and N. Barkai. *Nature*, 419:304, 2002.
- [10] T. Bollenbach, K. Kruse, P. Pantazis, M. González-Gaitán, and F. Jülicher. *Phys. Rev. Lett.*, 94:018103, 2005.
- [11] J. Jaeger, S. Surkova, M. Blagov, H. Janssens, D. Kosman, K.N. Kozlov, Manu, E. Myasnikova, C.E. Vanario-Alonso, M. Samsonova, D.H. Sharp, and J. Reinitz. *Nature*, 430:368, 2004.
- [12] A. Ochoa-Espinosa, G. Yucel, L. Kaplan, A. Pare, N. Pura, A. Oberstein, D. Papatsenko, and S. Small. *Proc. Natl. Acad. Sci. USA*, 102:4960, 2005.
- [13] S. Small, A. Blair, and M. Levine. *EMBO J.*, 11:4047, 1992.
- [14] L. Bintu, N.E. Buchler, H.G. Garcia, U. Gerland, T. Hwa, J. Kondev, and R. Phillips. *Curr. Opin. Gen. Dev.*, 15:116, 2005.
- [15] A. Eldar, D. Rosin, B.-Z. Shilo, and N. Barkai. *Developmental Cell*, 5:635, 2003.
- [16] E. Ben-Naim and S. Redner. *J. Phys. A: Math. Gen.*, 25:L575, 1992.
- [17] M.D. Schroeder, M. Pearce, J. Fak, HQ Fan, U. Unnerstall, E. Emberly, N. Rajewsky, E.D. Siggia, and U. Gaul. *PLoS Biol.*, 2:e271, 2004.
- [18] E.M. Lucchetta, J.H. Lee, L.A. Fu, N.H. Patel, and R. F. Ismagilov. *Nature*, 434:1134, 2005.
- [19] P. R. ten Wolde. private communication.
- [20] M. Howard and P. R. ten Wolde. *Phys. Rev. Lett.*, 95:208103, 2005.
- [21] O. Crauk and N. Dostatni. *Curr. Biol.*, 15:1888, 2005.

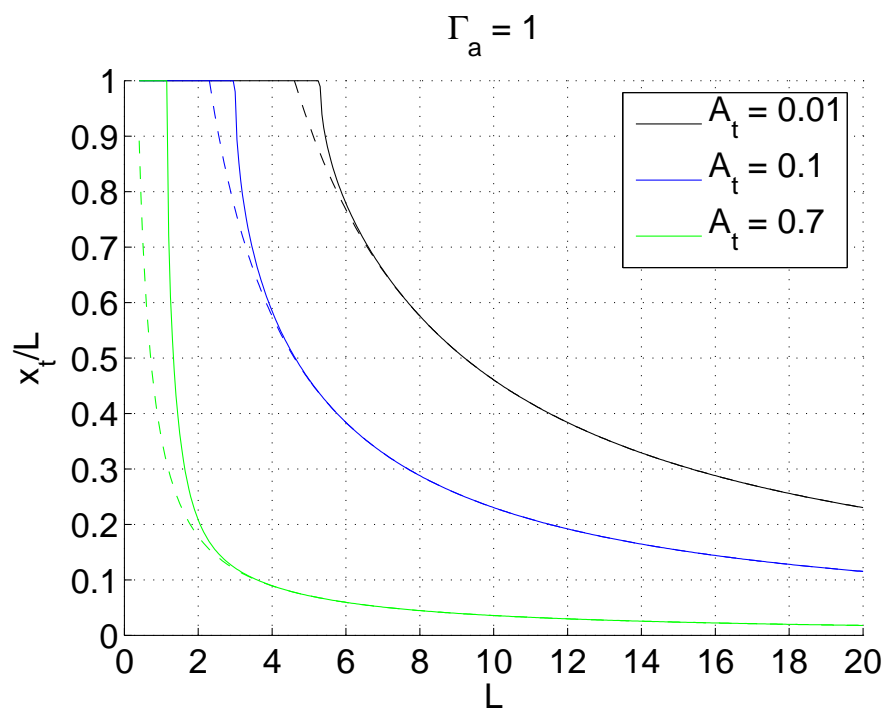


Figure 1. Dependence of normalised x_t on system length L for the case of a single gradient. The solid lines are the analytic expressions Eq. (4) for x_t/L for values of the threshold concentration equal to (from top to bottom) $A_t = 0.01, 0.1, 0.7$. Dashed lines are x_∞/L curves as given by Eq. (6). All parameters are unity unless otherwise stated.

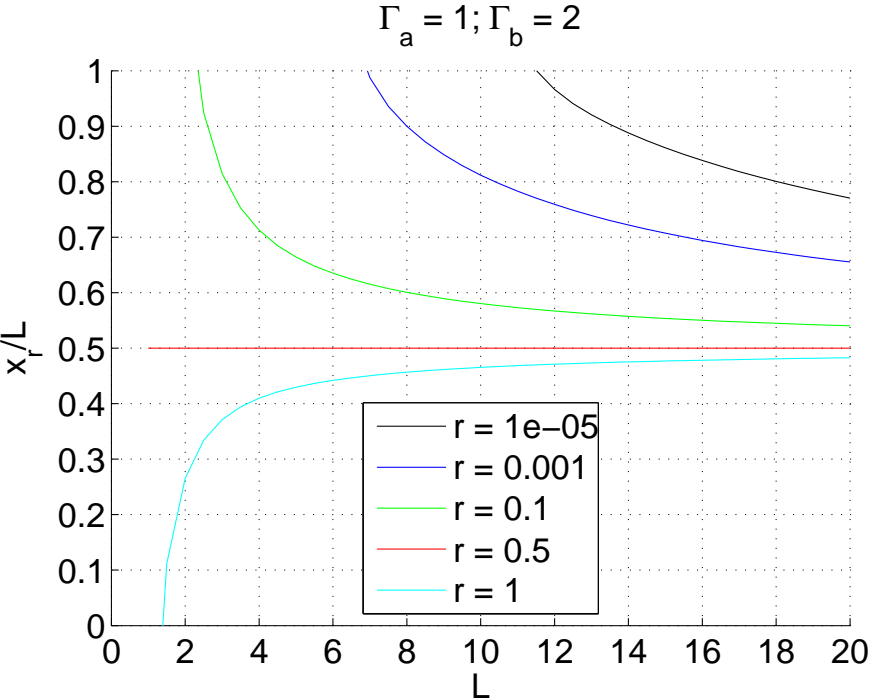


Figure 2. Dependence of normalised x_r on system length L in the combinatorial two-gradient model, as given by Eq. (13), for values of the threshold ratio equal to (from top to bottom) $r = 10^{-5}, 10^{-3}, 10^{-1}, 0.5, 1$. All parameters are unity unless otherwise stated.

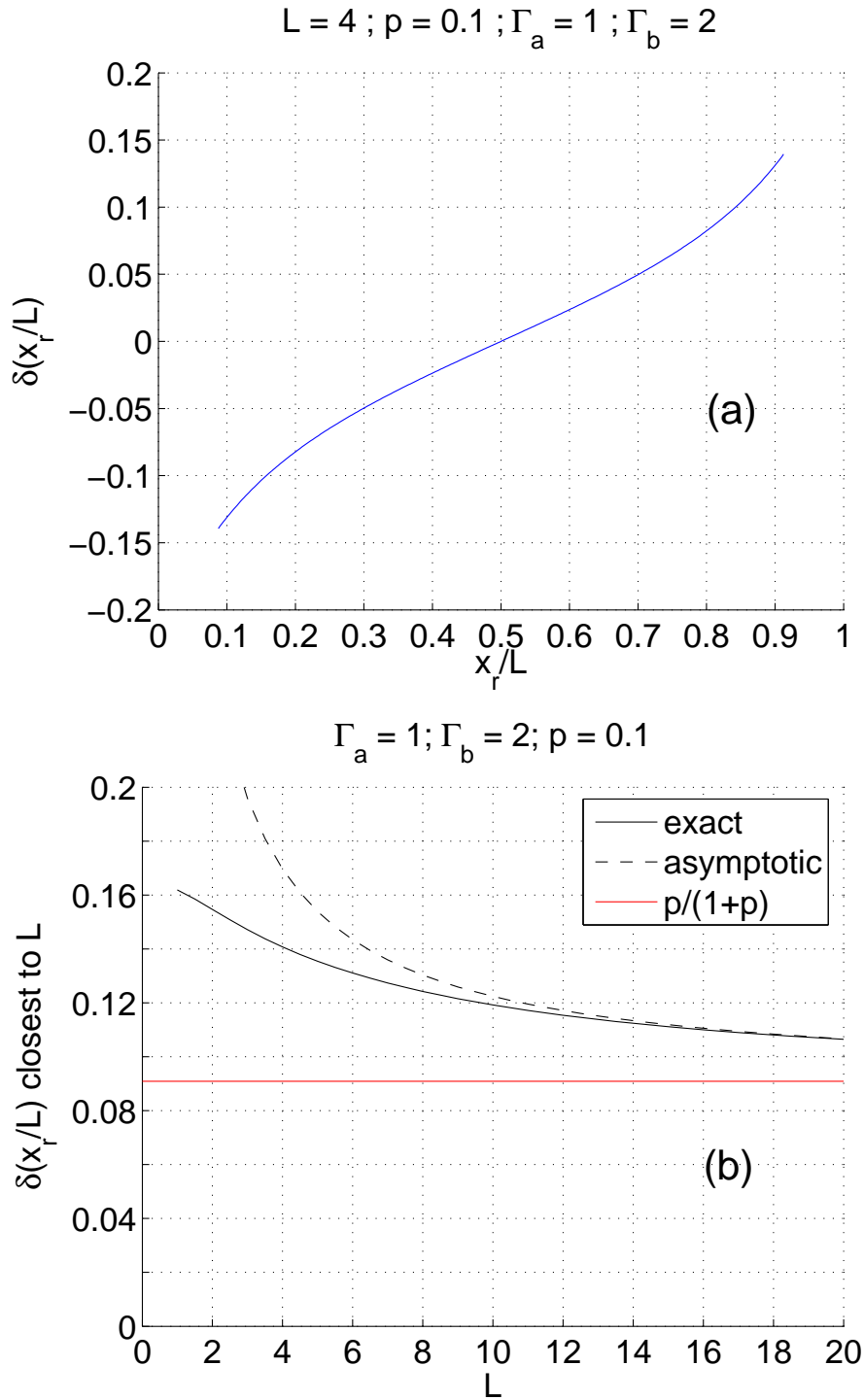


Figure 3. (a) Dependence of the variation $\delta(x_r/L)$ on normalised position x_r/L in the developing field for $L = 4$ and a percentage change in system size of 10%. (b) The variation $\delta(x_r/L)$ closest to the right boundary of the developing field as a function of L (solid line). At each L we have chosen the target gene whose threshold ratio r satisfies $L^*(r) = L - pL$. The variation in the fractional position at which this gene is turned on is then given by $\delta\left(\frac{x_r}{L}\right) = 1 - \frac{x_r(L+pL)}{L+pL}$. The dashed line is an asymptotic expression. The horizontal (red) line is the limiting value $p/(1+p)$ of the solid and dashed curves.

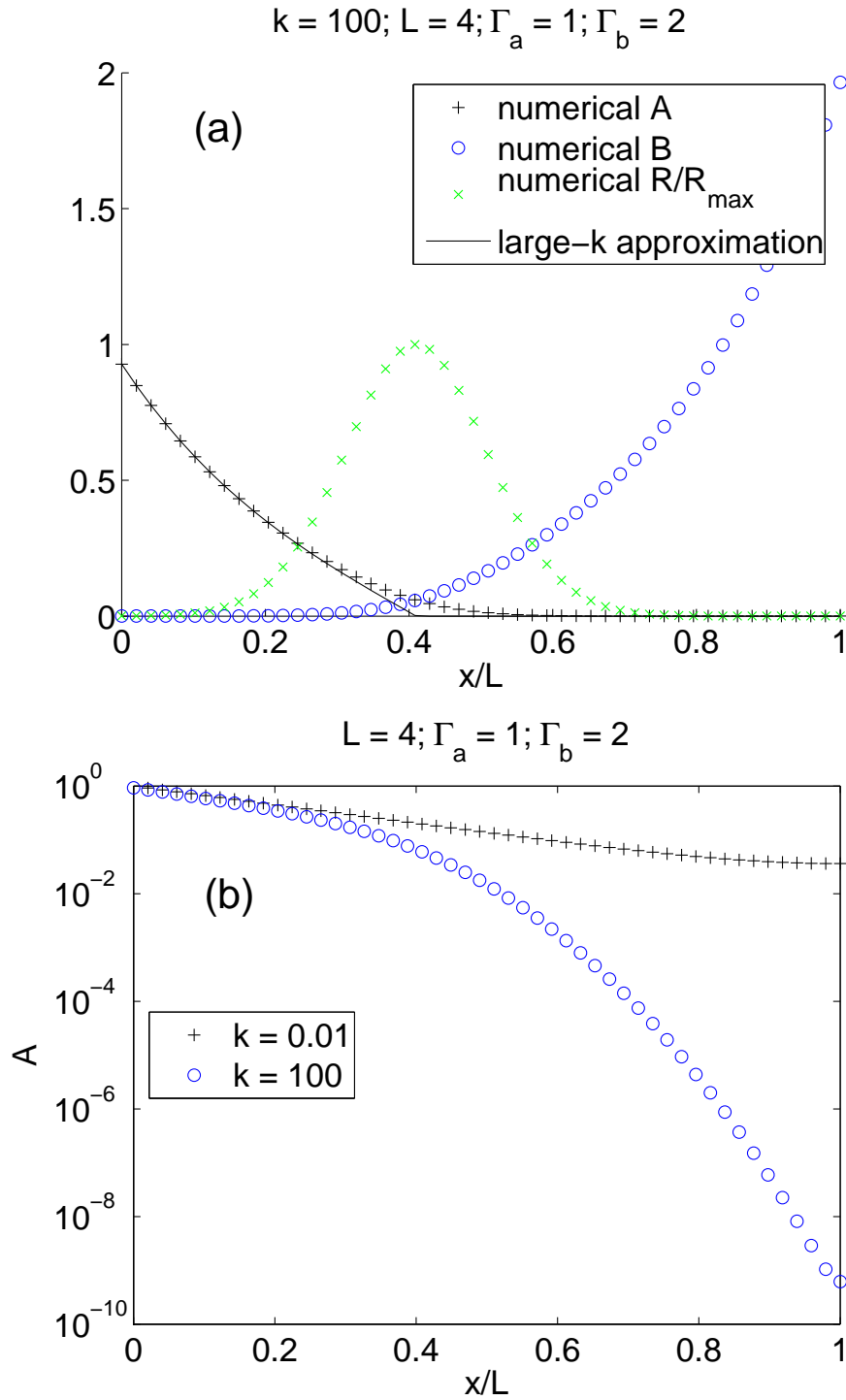


Figure 4. (a) Comparison of the high-annihilation-rate approximation (Eq. (21), solid line) with the numerical solution (circles) of the full annihilation model (Eqs. (16) and (17)). The annihilation zone is the reaction front $R(x) = kA(x)B(x)$. All parameters are unity unless otherwise stated. (b) $A(x)$ plotted on a logarithmic scale in the cases $k = 0.01$ and $k = 100$. Note the crossover from slow decay in the A -rich region to fast decay in the B -rich region in the case $k = 100$. All parameters are unity unless otherwise stated.

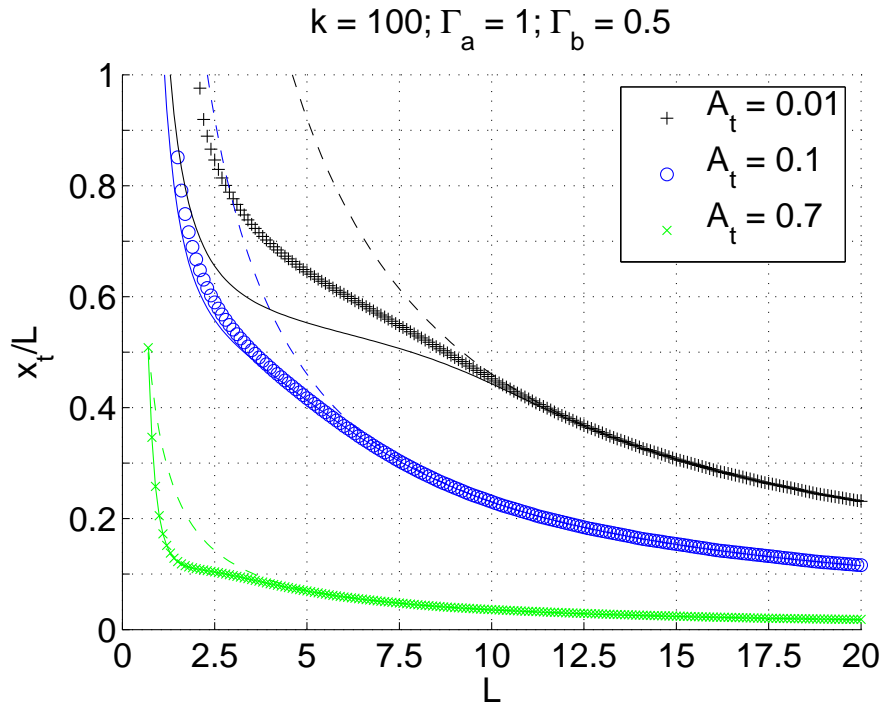


Figure 5. Dependence of normalised x_t on system length L with $k = 100$ and $\Gamma_b < \Gamma_a$. The plus signs, circles and crosses are numerical solutions of Eqs. (16) and (17) for values of the threshold concentration equal to (from top to bottom) $A_t = 0.01, 0.1, 0.7$. The solid lines are the corresponding analytic expressions Eq. (26) obtained in the high-annihilation-rate limit. Dashed lines are x_∞/L curves as given by Eq. (6). All parameters are unity unless otherwise stated.

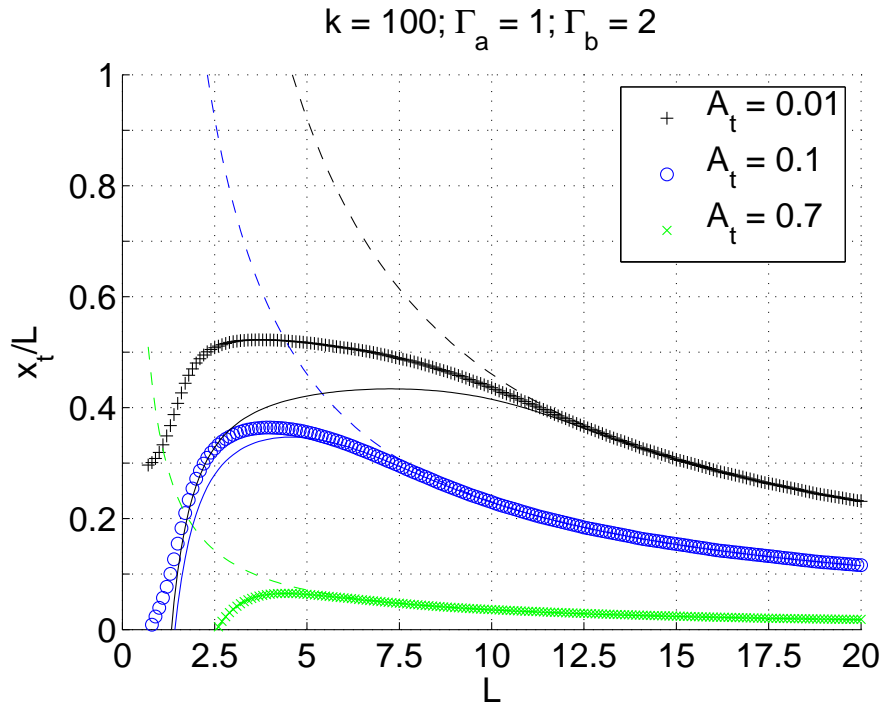


Figure 6. Dependence of normalised x_t on system length L with $k = 100$ and $\Gamma_b > \Gamma_a$. The plus signs, circles and crosses are numerical solutions of Eqs. (16) and (17) for values of the threshold concentration equal to (from top to bottom) $A_t = 0.01, 0.1, 0.7$. The solid lines are the corresponding analytic expressions Eq. (26) obtained in the high-annihilation-rate limit. Dashed lines are x_∞/L curves as given by Eq. (6). All parameters are unity unless otherwise stated.

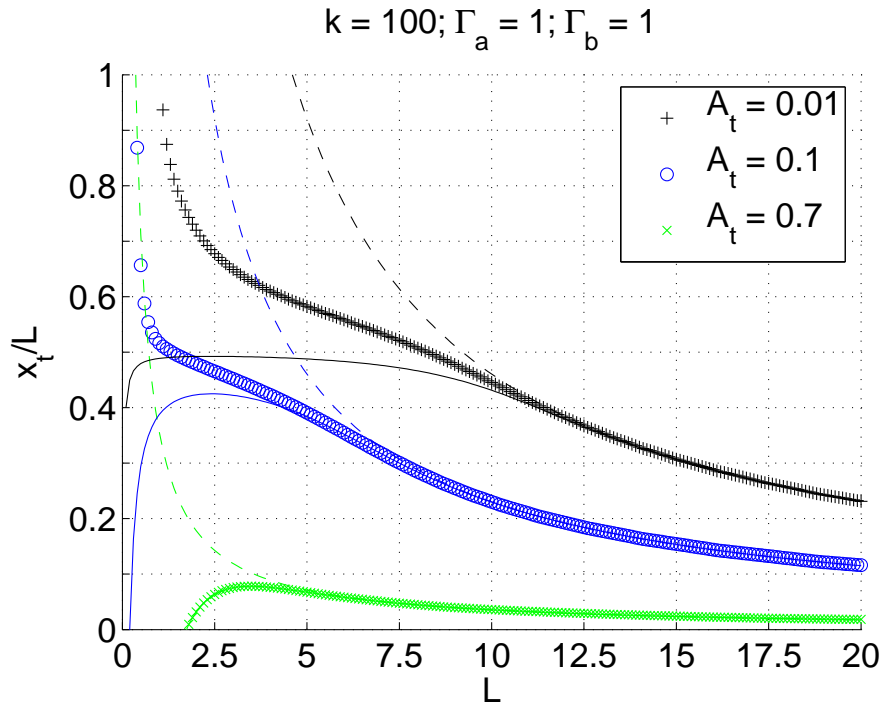


Figure 7. Dependence of normalised x_t on system length L with $k = 100$ and $\Gamma_b = \Gamma_a$. The plus signs, circles and crosses are numerical solutions of Eqs. (16) and (17) for values of the threshold concentration equal to (from top to bottom) $A_t = 0.01, 0.1, 0.7$. The solid lines are the corresponding analytic expressions Eq. (26) obtained in the high-annihilation-rate limit. Dashed lines are x_∞/L curves as given by Eq. (6). All parameters are unity unless otherwise stated.

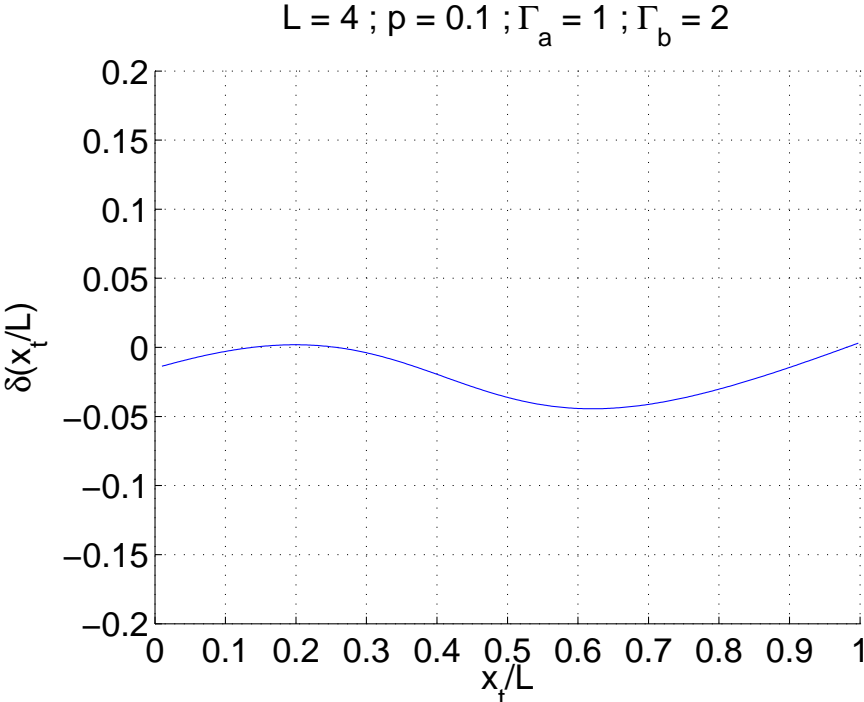


Figure 8. The dependence of the variation $\delta(x_t/L)$ on normalised position x_t/L in the high-annihilation-rate approximation of the annihilation model. Positions to the left of x_e are set by the A gradient while positions to the right are set by the B gradient. All parameters are unity unless otherwise stated.

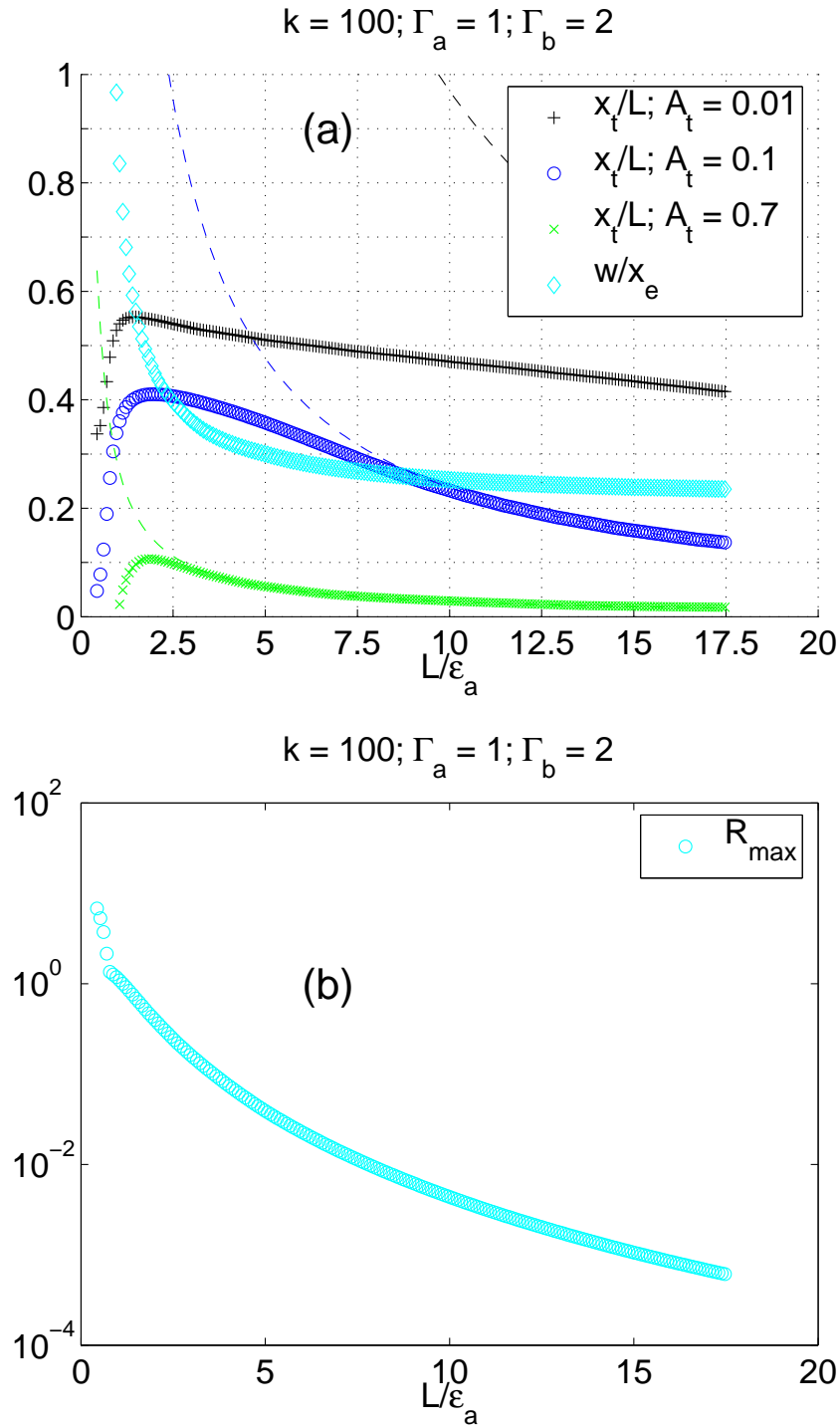


Figure 9. (a) Dependence of normalised x_t on system length L in the case of quadratic degradation. The plus signs, circles and crosses are numerical solutions of the full annihilation model for values of the threshold concentration equal to (from top to bottom) $A_t = 0.01, 0.1, 0.7$. The dashed lines are x_∞/L curves as given by Eq. (30). Also shown (cyan diamonds) is the ratio of the full width at half maximum w to the comparison point x_e . (b) The dependence of the amplitude R_{max} of the local annihilation rate $R(x) = kA(x)B(x)$ on system length L . In (a) and (b) all parameters are unity unless otherwise stated.

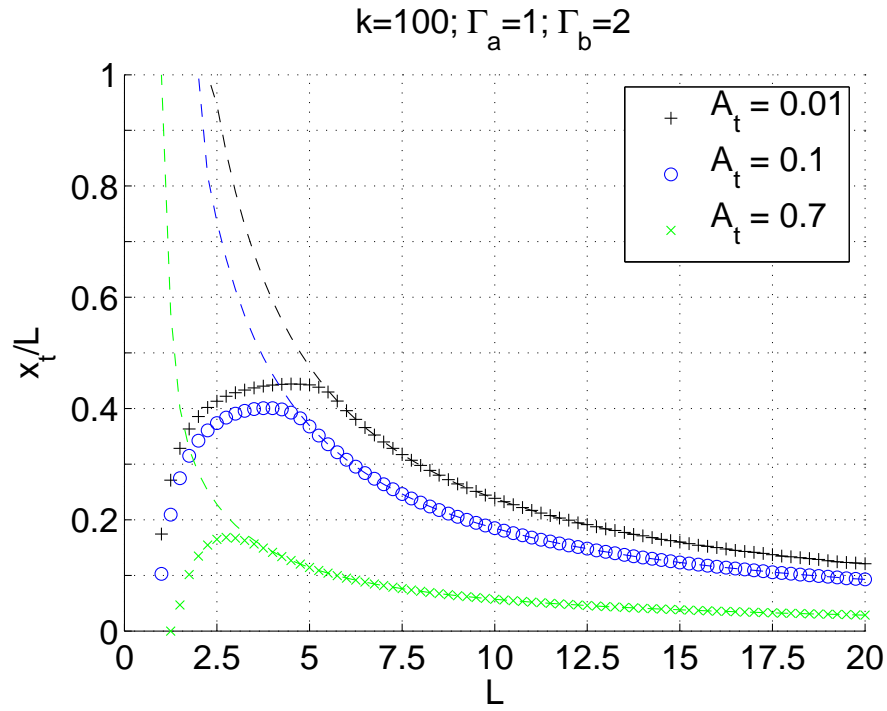


Figure 10. Dependence of scaled threshold position x_t/L on system length L in the simplest case of nonlinear diffusion, $D_a = \delta_a A$ and $D_b = \delta_b B$. The degradation terms are linear. The plus signs, circles and crosses are numerical solutions of the full annihilation model for values of the threshold concentration equal to (from top to bottom) $A_t = 0.01, 0.1, 0.7$. Dashed lines are corresponding curves in the case $k = 0.01$. All parameters are unity unless otherwise stated.

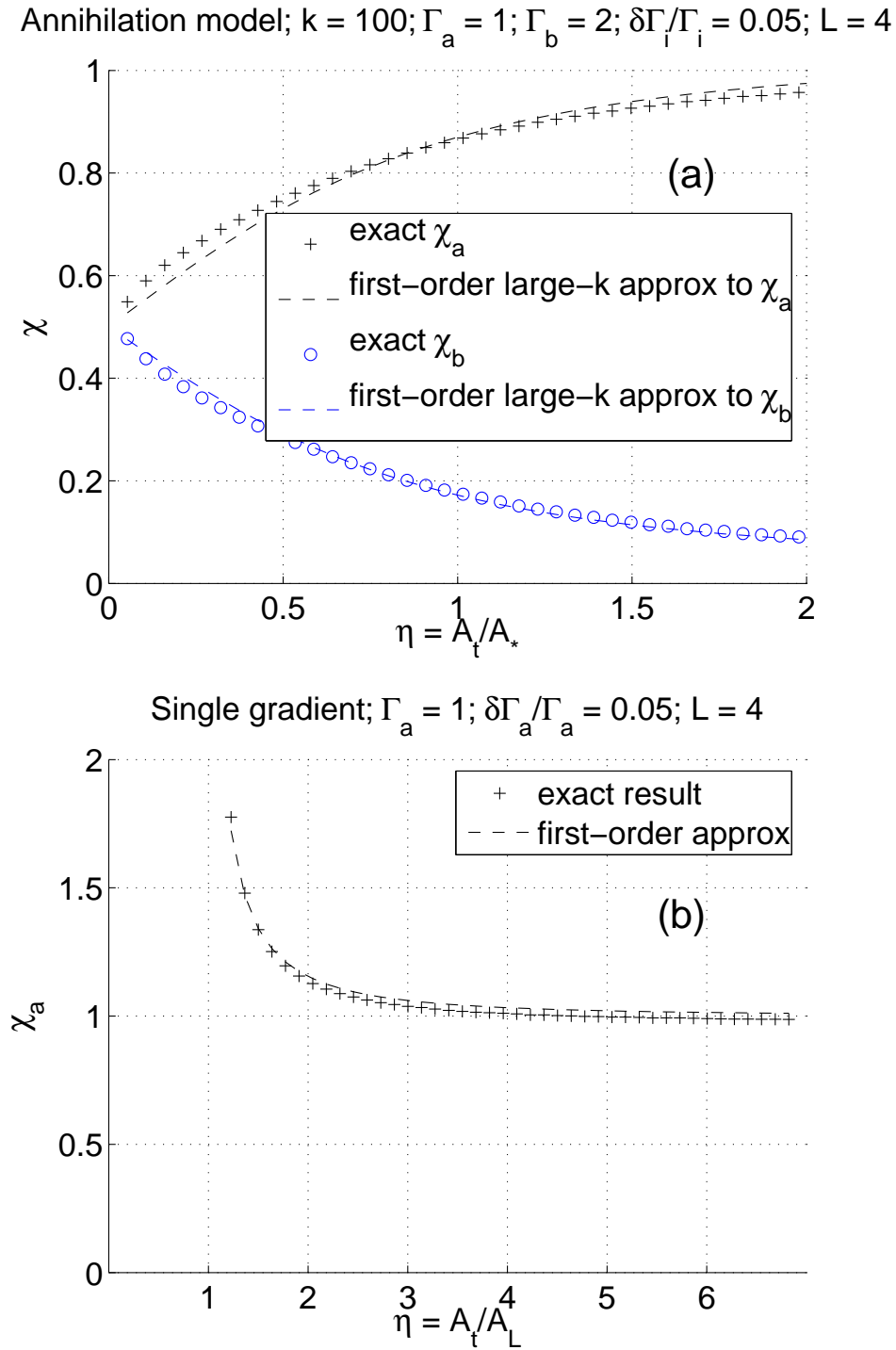


Figure 11. Sensitivity of the threshold position x_t to infinitesimal variations in the source fluxes Γ_a and Γ_b in (a) the annihilation model (constant diffusion constant and linear degradation) and (b) the single-gradient model. The coefficient of variation χ_i is defined by Eq. (32) in the text. The data plotted as plus signs and circles were obtained by solving numerically the full model, while the dashed lines represent (from top to bottom) Eqs. (33), (34) and (35). All parameters are unity unless otherwise stated.